

We are IntechOpen, the world's leading publisher of Open Access books Built by scientists, for scientists

6,900

Open access books available

186,000

International authors and editors

200M

Downloads

Our authors are among the

154

Countries delivered to

TOP 1%

most cited scientists

12.2%

Contributors from top 500 universities



WEB OF SCIENCE™

Selection of our books indexed in the Book Citation Index
in Web of Science™ Core Collection (BKCI)

Interested in publishing with us?
Contact book.department@intechopen.com

Numbers displayed above are based on latest data collected.
For more information visit www.intechopen.com



Effect of Transition Metal on Structural and Dielectric Properties of $\text{Mg}_{0.5}\text{Tm}_{0.5}\text{Fe}_2\text{O}_4$ (Tm = Zn and Cu) System

Pallavi Saxena and Anand Yadav

Abstract

This study explored the structural and dielectric features of $\text{Mg}_{0.5}\text{Tm}_{0.5}\text{Fe}_2\text{O}_4$ (Tm = Zn and Cu) that were synthesized by the Solid-state reaction (SSR) method. The X-ray powder diffraction (XRD) analysis reveals that the prepared samples are single-phase cubic structure without any impurity. Rietveld-refined X-ray diffraction results reveal the formation of cubic structure and all the peaks of $\text{Mg}_{0.5}\text{Zn}_{0.5}\text{Fe}_2\text{O}_4$ and $\text{Mg}_{0.5}\text{Cu}_{0.5}\text{Fe}_2\text{O}_4$ are perfectly indexed in the cubic ($Fd-3m$) structure. Dielectric constant and dielectric loss variation with frequency were also explored. Both decrease when the relevant alternating field is increasing and become constant at high frequencies which reflects the important role of interfacial polarization. Furthermore, the $\text{Mg}_{0.5}\text{Cu}_{0.5}\text{Fe}_2\text{O}_4$ having the smallest crystallite size (~ 44.73 nm) has a high dielectric constant ($\sim 4.41 \times 10^4$) value as compare to $\text{Mg}_{0.5}\text{Zn}_{0.5}\text{Fe}_2\text{O}_4$.

Keywords: solid-state synthesis, ferrite, crystallite size, X-ray diffraction, dielectric properties

1. Introduction

Ferrites are insulating magnetic oxides with high electrical resistance, low dielectric losses, high permeability, and high saturation magnetization. These magnetic materials are special and can be used in several device applications. Transition metal ion-doped spinel ferrites are fascinating due to high dielectric constant and low dielectric losses [1, 2]. Soft ferrite materials such as Mg-Zn ferrites have vast technological importance due to their relatively high Curie temperature, low cost, and eco-friendly stable nature. The transport properties of soft ferrites are mainly controlled by divalent impurities. Further, soft ferrites are used in advanced technologies such as magnetic resonance imaging (MRI), magnetic drug delivery, microwave absorbers, catalysis, detoxification of biological fluids, transformer cores, magnetically controlled transport of anti-cancer drugs, sensors [2].

Spinel ferrites with formula AB_2O_4 (A = Mg, Zn, Cu) have a cubic structure with an $Fd3m$ space group. However, MgFe_2O_4 is having an inverse spinel structure with zero magnetic moments. This inversion is usually affected by the temperature given during calcination, while ZnFe_2O_4 often has a normal spinel structure without

magnetic moment. Due to low Neel temperature both the ferrites show antiferromagnetic characteristics. It shows paramagnetic behavior due to weak superexchange interaction at room temperature [3, 4]. The polycrystalline Mg-Zn inverse spinel ferrites are commonly represented by $(\text{Zn}_x\text{Mg}_y\text{Fe}_{1-x-y})[\text{Mg}_{1-x-y}\text{Fe}_{1+x+y}]\text{O}_4$, where Zn^{2+} ions are bound to the tetrahedral sites (interstitial) and Mg^{2+} ion occupy the B sites [octahedral] ions have an affinity towards the interstitial (tetrahedral) site and Mg^{2+} ions occupy octahedral sites. However, Fe^{3+} ions occupied at both the tetrahedral and octahedral sites [5]. The effect of Cu ion doping on Mg-Zn ferrites should be investigated as the copper ferrites possess a tetragonal structure and Mg-Zn ferrites retain the spinel structure [6].

The materials having high dielectric constant and low dielectric losses are useful in microwave devices that make transition metal and rare earth doped Mg-Zn ferrite an attractive candidate. The dielectric properties are largely influenced by the method of synthesis, chemical structure, doping concentration, grain structure, calcination temperature, and the size of the dopant [7]. The previous studies have provided important findings on the frequency-dependent dielectric properties as the value of dielectric constant for MgFe_2O_4 is 57.93 at 10 Hz [8], for ZnFe_2O_4 is 2641 at 1 kHz [9], for $\text{Mg}_{0.75}\text{Zn}_{0.25}\text{Fe}_2\text{O}_4$ is 740 at 100 Hz and for $\text{Mg}_{0.5}\text{Zn}_{0.5}\text{Fe}_2\text{O}_4$ is near to ~50 at 100 Hz [4] whereas the dielectric constant of all these materials decreases with an increase in the frequency.

We have to use the solid-state reaction method to synthesize the $\text{Mg}_{0.5}\text{Tm}_{0.5}\text{Fe}_2\text{O}_4$ (Tm = Zn and Cu) ferrites. The key benefits of solid state reaction synthesis over other methods are that it is simple, cheaper, and convenient. It also requires less solvent, reduces contamination, and gives high yields of products. The present chapter mainly focuses on the crystal as well as the dielectric response of $\text{Mg}_{0.5}\text{Tm}_{0.5}\text{Fe}_2\text{O}_4$ (Tm = Zn and Cu) ferrite. The techniques used for the characterization of $\text{Mg}_{0.5}\text{Tm}_{0.5}\text{Fe}_2\text{O}_4$ (Tm = Zn and Cu) are X-ray diffraction (XRD) and dielectric measurements.

2. Experimental details

The $\text{Mg}_{0.5}\text{Tm}_{0.5}\text{Fe}_2\text{O}_4$ (Tm = Zn and Cu) samples were synthesized using a Solid-state reaction technique. All chemicals used here were of analytical grade without any further purification. Precursors such as zinc oxide (ZnO), magnesium oxide (MgO), ferric oxide (Fe_2O_3), and CuO (copper oxide) with 99.9% purity were combined in stoichiometric amounts and thoroughly mixed using a mortar pestle. The resulting powder was calcined in a muffle furnace open to the air at 1000 °C for 12 hours creating a solid sample that was again ground with mortar and pestle into a fine powder. The sample was reground and calcined again for 12 h at 1050 °C to increase the homogeneity of the prepared samples. Each heat treatment included a heating and cooling rate of 10 °C/min and with intermediate grindings. Further, an organic binder called polyvinyl acetate (PVA) is added to the powder sample to binds the particles. The obtained powder samples were compressed in the circular shape of 1 mm thick and 10 mm diameter pellets using a hydraulic press following the application of 8 tons of pressure. At last, the pellets were fully sintered at 1200 °C for 12 h, then steadily cooled to room temperature.

The X-ray diffraction patterns of the $\text{Mg}_{0.5}\text{Tm}_{0.5}\text{Fe}_2\text{O}_4$ (Tm = Zn and Cu) were recorded at ambient conditions using a Bruker D8 advanced diffractometer with a copper anode (1.5460 Å) in Bragg–Brentano geometry. This equipment possesses a LynxEye detector based on the silicon drift detector technique. The X-ray diffraction patterns were obtained in the 2θ angle range from 20 to 80°, using a step size

of 0.02° . The powder-diffraction data was processed by Rietveld refinements using the FullPROF program [10]. The dielectric properties of these samples have been tested in the impedance analyzer with the model-Novo control tech Germany alpha ATB, which is usable within the frequency range of $3 \mu\text{Hz}$ -20 MHz and the *ac* voltage range from 100 mV to 3 V. The high temperature silver paste was used on their two major surfaces for dielectric measurements.

3. Results and discussion

3.1 Structural analysis

A powder X-ray diffraction (XRD) analysis was used to determine the crystallinity and purity of prepared samples. The room temperature XRD pattern with indexed hkl for the prepared samples of $Mg_{0.5}Tm_{0.5}Fe_2O_4$ ($Tm = Zn$ and Cu , and henceforth designated as $Mg_{0.5}Zn_{0.5}Fe_2O_4$ and $Mg_{0.5}Cu_{0.5}Fe_2O_4$, respectively) samples are depicted in **Figure 1**. The XRD pattern of $Mg_{0.5}Zn_{0.5}Fe_2O_4$ indicates the presence of a single-phase, whereas the $Mg_{0.5}Cu_{0.5}Fe_2O_4$ sample shows minor impurity peaks which is due to the presence of minor secondary phase corresponds to unreacted monoclinic CuO phase (space group $C2/c$).

The observed diffracted peaks support the formation of a cubic spinel-type structure with the space group $Fd-3m$ and all the diffracted peaks are compared with the Joint Committee on Powder Diffraction Standards (JCPDS) data and match well with the Card No. 86-2267 [5]. The magnified view of the most pronounced peak (311) of $Mg_{0.5}Zn_{0.5}Fe_2O_4$ and $Mg_{0.5}Cu_{0.5}Fe_2O_4$ samples are shown in the inset of **Figure 1**. We observe that there is a slight shift occurring for each intensity peak as compared to $Mg_{0.5}Zn_{0.5}Fe_2O_4$ towards the higher angle side. This shifting is taking place due to the minor difference in the ionic radii of Cu^{2+} (0.72 \AA) and Zn^{2+} (0.74 \AA) ions.

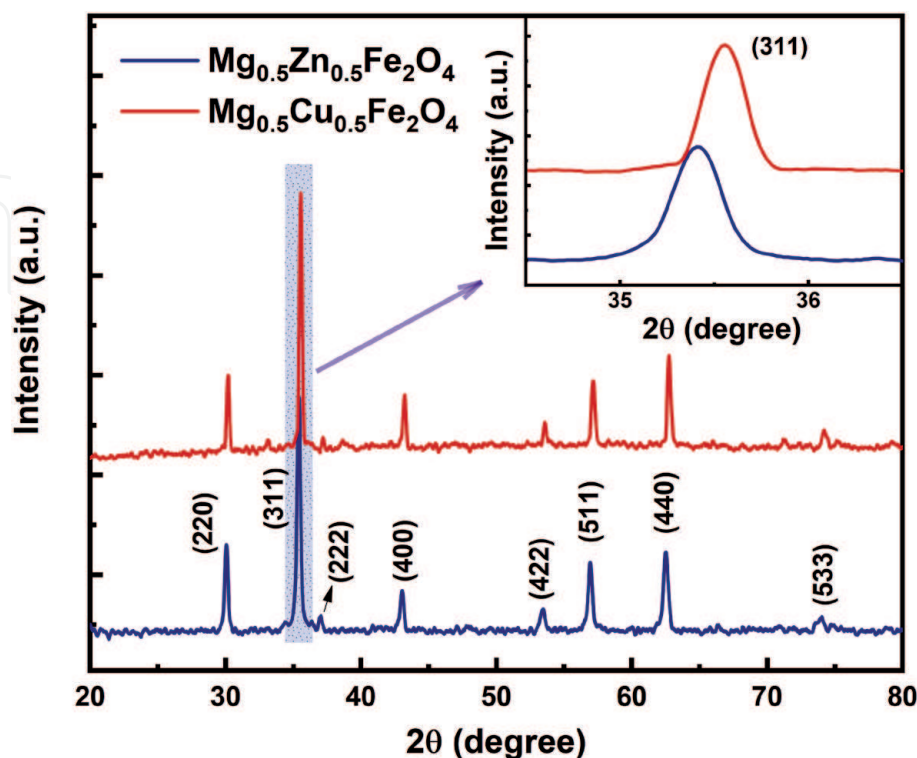


Figure 1.
XRD patterns of $Mg_{0.5}Tm_{0.5}Fe_2O_4$ ($Tm = Zn$ and Cu) ferrites.

The observed diffracted peaks support the formation of a cubic spinel-type structure with the space group $Fd\bar{3}m$ and all the diffracted peaks are compared with the Joint Committee on Powder Diffraction Standards (JCPDS) data and match well with the Card No. 86-2267 [5]. The magnified view of the most pronounced peak (311) of $\text{Mg}_{0.5}\text{Zn}_{0.5}\text{Fe}_2\text{O}_4$ and $\text{Mg}_{0.5}\text{Cu}_{0.5}\text{Fe}_2\text{O}_4$ samples are shown in the inset of **Figure 1**. We observe that there is a slight shift occurring for each intensity peak as compared to $\text{Mg}_{0.5}\text{Zn}_{0.5}\text{Fe}_2\text{O}_4$ towards the higher angle side. This shifting is taking place due to the minor difference in the ionic radii of Cu^{2+} (0.72 Å) and Zn^{2+} (0.74 Å) ions.

The Debye Scherrer's (DS) and the Williamson – Hall (WH) techniques were used to calculate the crystallite size (t). In the DS method, the average crystallite size was estimated using the Scherrer's Equation [4] $t = 0.9\lambda/\beta\cos\theta$, where β is full width at half maximum (FWHM), λ is the wavelength of X-ray employed, and θ is the diffraction angle. For $\text{Mg}_{0.5}\text{Zn}_{0.5}\text{Fe}_2\text{O}_4$ and $\text{Mg}_{0.5}\text{Cu}_{0.5}\text{Fe}_2\text{O}_4$, the measured values for crystallite sizes using DS are ~30.12 and 25.59 nm respectively. In the WH method, a plot of $\beta \cos\theta$ against $4 \sin\theta$ is plotted as shown in **Figure 2**. The slope thus represents strain and the y-intersect of the fitted line represents crystallite size.

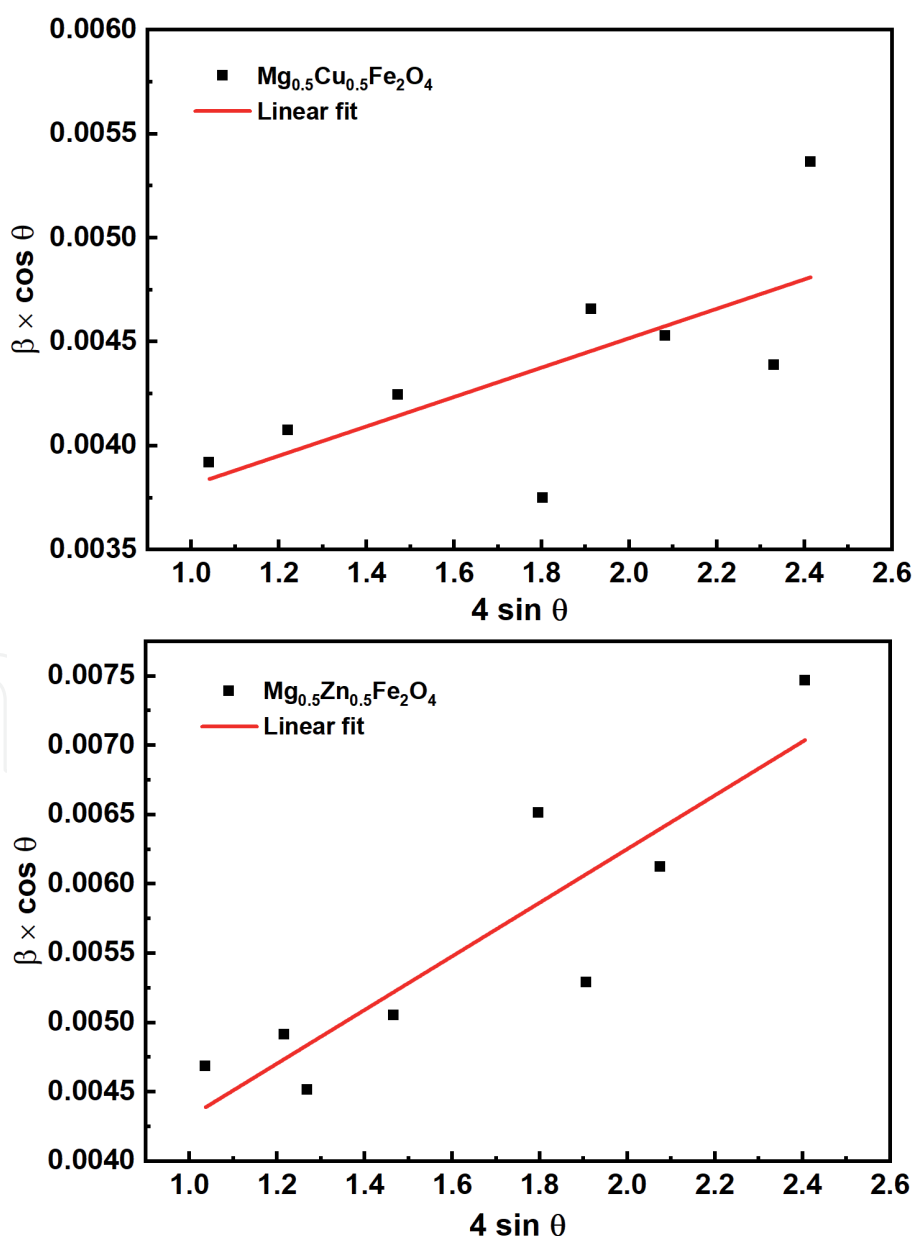


Figure 2. Williamson–Hall (WH) plot of $\text{Mg}_{0.5}\text{Tm}_{0.5}\text{Fe}_2\text{O}_4$ ($\text{Tm} = \text{Zn}$ and Cu) ferrites.

The average crystallite size calculated by the WH method ranges from ~58.26 to 44.73 nm, which is dependent on the broadening of peaks with doping concentration [11]. The calculated value of crystallite size, dislocation densities, and microstrain for $Mg_{0.5}Zn_{0.5}Fe_2O_4$ and $Mg_{0.5}Cu_{0.5}Fe_2O_4$ samples, are tabulated in **Table 1**. Furthermore, the dislocation density (δ) gives further insight into the number of crystal defects. It is seen that the value of dislocation density decreases for $Mg_{0.5}Cu_{0.5}Fe_2O_4$ which implies the reduction in the defects and dislocation. It should be noticed that the microstrain of $Mg_{0.5}Cu_{0.5}Fe_2O_4$ is significantly smaller than the microstrain of $Mg_{0.5}Zn_{0.5}Fe_2O_4$ and it is consistent with the larger average crystal size of $Mg_{0.5}Zn_{0.5}Fe_2O_4$ (as evident in **Table 1**).

Rietveld refinements of XRD (FullPROF software) results are shown in **Figure 3**, which confirm that $Mg_{0.5}Zn_{0.5}Fe_2O_4$ and $Mg_{0.5}Cu_{0.5}Fe_2O_4$ compounds crystallize with an $Fd-3m$ space group in a cubic form [12]. The pseudo-voigt analytical function is used to fit the experimental result of XRD. The structural cell parameters and refinement factors are listed in **Table 2**. The strongest reflection in both the samples comes from the (311) plane that indicates both the samples have the spinel phase. Fundamental reflections from the crystal planes (220), (311), (222), (400), (422), (511), (440), and (533), characterizing the spinel ferrites are identified.

It is observed that the lattice parameters slightly decreases for $Mg_{0.5}Cu_{0.5}Fe_2O_4$. The refined values of lattice parameters are $a = 8.3932 \text{ \AA}$ for $Mg_{0.5}Zn_{0.5}Fe_2O_4$ and $a = 8.3679 \text{ \AA}$ for $Mg_{0.5}Cu_{0.5}Fe_2O_4$. These parameters are consistent with the previously reported results [13]. The slight variation in the lattice parameters may be related to the anion–cation distance for the interstitial A- and B-site in the spinel structure, which could be correlated with the fraction of Mg^{2+} , Fe^{3+} , and Zn^{3+} ions among these sites directly. The decrease in lattice constant with an increase in the copper concentration may be attributed to the smaller ionic radius of Cu^{2+} (0.72 \AA) compared with that of Zn^{2+} (0.74 \AA) ion [14]. Indeed, a variation of lattice parameters involves a variation in 2θ , we can say that this shift of the peaks influences the lattice parameters of the structure.

3.2 Dielectric studies

The value of the dielectric constant (ϵ') is calculated using $\epsilon' = C_p d / \epsilon_0 A$, where, C_p is the measured value of the capacitance, d is the thickness of the pellet, ϵ_0 is the permittivity of free space and A is the area of cross-section of the pellet. **Figure 4** indicates the variation in the dielectric constant as a function of the frequency at room temperature between 1 kHz and 10 MHz. It is observed that for both samples the dielectric constant decreases with an increase in frequency and becomes constant at a higher frequency. The reduction in the dielectric constant values can be caused by electron exchange interaction between Fe^{2+} and Fe^{3+} ions, which does not obey the alternating electric field. The decrease of dielectric constant with the increase of frequency is observed in the case of Mg-Zn ferrite. Similar behavior was

Samples	Average crystallite size using SM (in nm)	Average crystallite size using WHM (in nm)	Micro strain $\epsilon \times 10^{-3}$ (lines/m ⁴)	Dislocation density $\delta \times 10^{14}$ (lines/m ²)
$Mg_{0.5}Zn_{0.5}Fe_2O_4$	30.12	58.26	3.16	2.95
$Mg_{0.5}Cu_{0.5}Fe_2O_4$	25.59	44.73	3.08	4.98

Table 1. Average crystallite size using SM and WHM, micro strain (ϵ) and dislocation density (δ) derived from X-ray diffraction data.

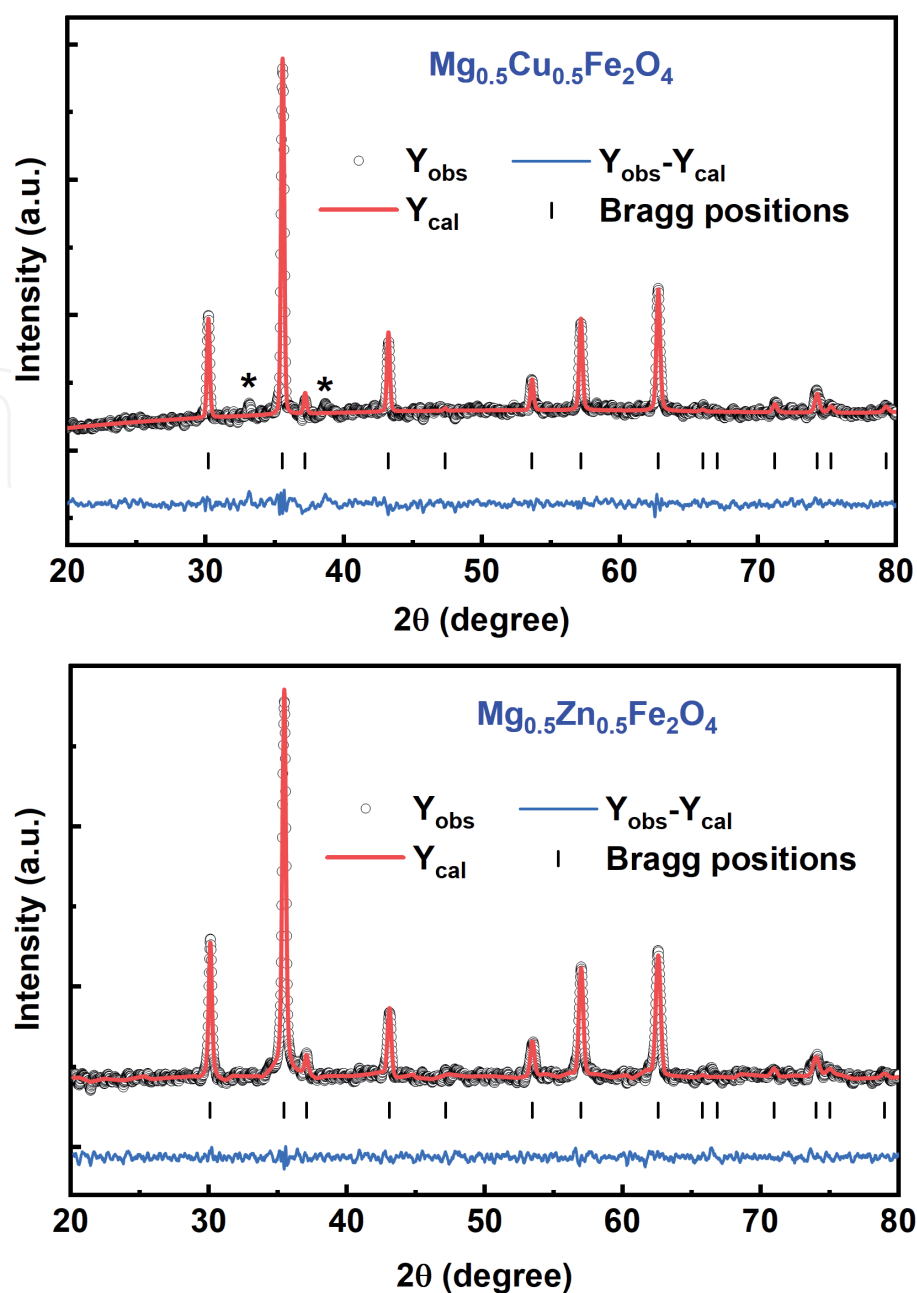


Figure 3. Rietveld refinement fitting results of the X-ray powder diffraction patterns of $Mg_{0.5}Tm_{0.5}Fe_2O_4$ ($Tm = Zn$ and Cu) ferrites.

Parameters	Samples	
	$Mg_{0.5}Zn_{0.5}Fe_2O_4$	$Mg_{0.5}Cu_{0.5}Fe_2O_4$
2θ range (deg.)	$20^\circ - 80^\circ$	$20^\circ - 80^\circ$
Step size (deg.)	0.02°	0.02°
Wavelength	1.5406 \AA	1.5406 \AA
Space group	$Fd-3m$	$Fd-3m$
a (\AA)	8.3932	8.3679
R_{wp}	12.9	14.5
χ^2	1.82	1.65

Table 2. Details of Rietveld refined XRD parameters for $Mg_{0.5}Tm_{0.5}Fe_2O_4$ ($Tm = Zn$ and Cu).

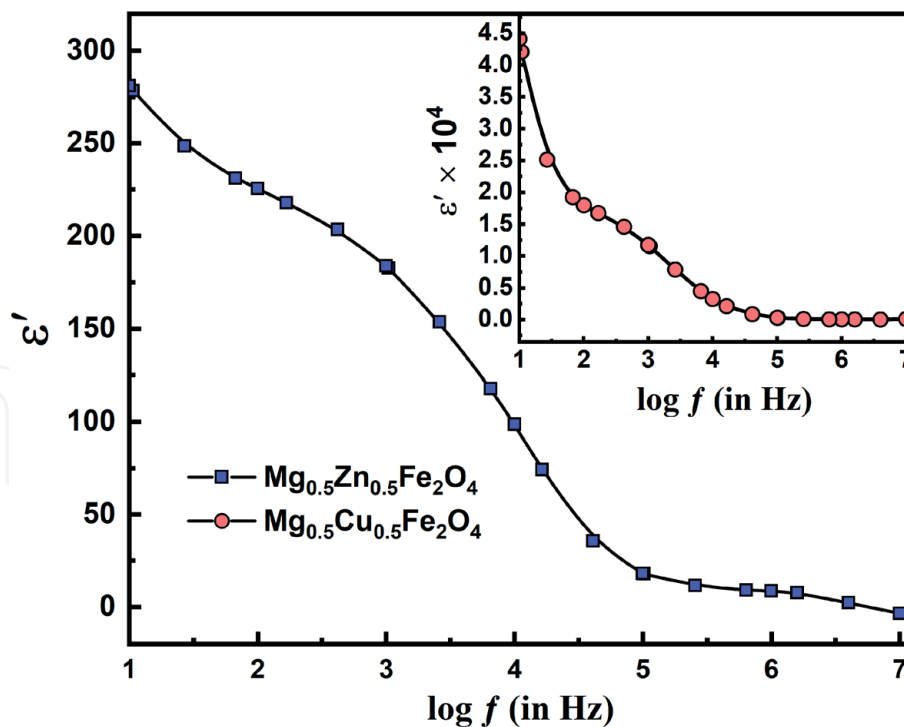


Figure 4.
 Frequency dependent dielectric constant (ϵ') of $Mg_{0.5}Tm_{0.5}Fe_2O_4$ ($Tm = Zn$ and Cu) ferrites.

also observed in other ferrite systems [4, 15]. The reduction in the dielectric constant with an increased frequency is a normal dielectric behavior of spinel ferrites and can be described by the dipole relaxation phenomenon. Dipole relaxation refers to the relaxation response of a dielectric medium to an external electric field. In general, relaxation is a delay in the response of a system. It is well known that in the heterogeneous structure the samples consist of well-conducting grains separated by poorly conducting grain boundaries [16]. If the resistance of the grain boundary is high enough, the electrons are pile up at the grain boundary and produce polarization. However, the electrons reverse their direction of motion more frequently, as the frequency of the applied field is changes. This reduces the probability of electrons reaching the grain boundary and thereby decreases polarization. Thus, the dielectric constant decreases with the increasing frequency of the applied field [17].

Also from **Figure 4**, it is quite clear that the value of the dielectric constant is higher for $Mg_{0.5}Cu_{0.5}Fe_2O_4$ and is found to be ~ 44140 , which is much higher as compared to ~ 281 obtained for the $Mg_{0.5}Zn_{0.5}Fe_2O_4$. This increase in the dielectric constant ϵ' can be explained based on the mechanism of the polarization process. The origin of polarization is due to the influence of the size mismatch of the cations. The coexistence of multiple phases requires that the strain energies of the domains at the boundaries should be comparable. Since the different domains have different electronic properties, they can give rise to large dielectric constants. The whole polarization in ferrites is primarily due to the space charge polarization, the conductivity in materials, and the hopping exchange of the charges between two localized states. Thus the dielectric constant decreases with an increase in frequency for both samples. It is worth mentioning here that the dielectric constant increases with an increase in Cu concentration [18].

In **Figure 5**, the variation of dielectric loss ($\tan \delta$) as a function of the logarithm of frequency is depicted. It can be seen in the figure that the dielectric loss of the $Mg_{0.5}Zn_{0.5}Fe_2O_4$ compound is very high and is found to decrease with 50% Cu doping concentration. Besides, the decline in $\tan \delta$ with the increase in frequency is following Koop's phenomenological model [19]. The dielectric loss arises when the

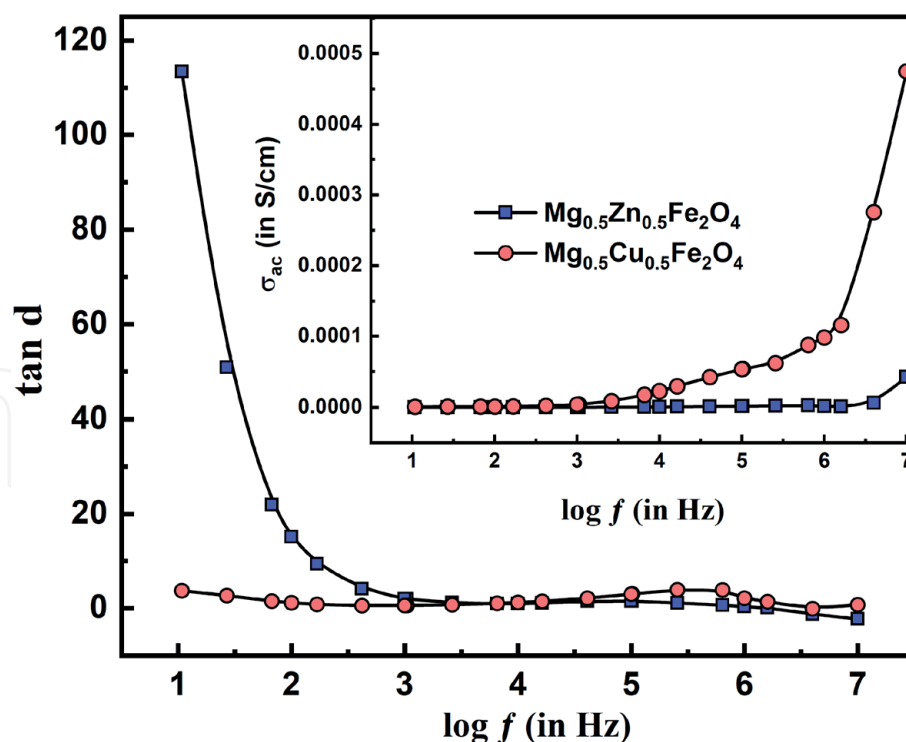


Figure 5. Frequency dependent dielectric loss ($\tan \delta$) and ac conductivity (σ_{ac}) of $Mg_{0.5}Tm_{0.5}Fe_2O_4$ ($Tm = Zn$ and Cu) ferrites.

polarization lags behind the applied alternating field and is caused by the presence of impurities and structural inhomogeneity. The value of dielectric loss tangent is very low in the higher frequency region. The frequency-dependent *ac* conductivity (σ_{ac}) variation of $Mg_{0.5}Tm_{0.5}Fe_2O_4$ ($Tm = Zn$ and Cu) samples are shown in the inset of **Figure 5**. In this study, *ac* conductivity is found to increase as the frequency of applied *ac* field increases for both the samples, because the increase in the frequency of *ac* applied field enhances the hopping of charge carriers. It is also evident from **Figure 5** that *ac* conductivity is initially low for $Mg_{0.5}Zn_{0.5}Fe_2O_4$ and found to enhance with doping of Cu ion $Mg_{0.5}Cu_{0.5}Fe_2O_4$ at high frequency. The improvement is due to both short-range hopping motion and long-range displacement of oxygen vacancies involved in the conduction mechanism. The replacement of Zn ion with Cu ion results in the generation of more oxygen vacancies and leading to an increase in the long-range conduction path to the charged defect, which in turn increases the conductivity of $Mg_{0.5}Cu_{0.5}Fe_2O_4$ [20].

The electrical modulus analysis is very useful to detect electrode polarization, grain boundary conduction effect, electrical conductivity, and bulk properties. This technique also provides an insight into the electrical processes occurring in the materials. The modulus plots of M' versus M'' for $Mg_{0.5}Zn_{0.5}Fe_2O_4$ and $Mg_{0.5}Cu_{0.5}Fe_2O_4$ are shown in **Figure 6**. The deformed semi-circles are formed in both samples. The $M'-M''$ plot of $Mg_{0.5}Zn_{0.5}Fe_2O_4$ shows two regions, the large semicircle was believed to be induced by the grain effect, due to the smaller capacitance value dominated in the electric modulus spectra. The presence of single semicircular arcs suggests the presence of only grain contributions in these types of materials. The $Mg_{0.5}Cu_{0.5}Fe_2O_4$ samples do not show any semi-circle type behavior, which suggests that only grain capacitance is dominant and the grain boundary modulus is beyond the measurement scale. It is based on the fact modulus plot highlights the phenomenon with small values of capacitance. It is difficult to obtain two full semicircles grain boundaries on the same scale in the impedance plot because of the huge difference in capacitive

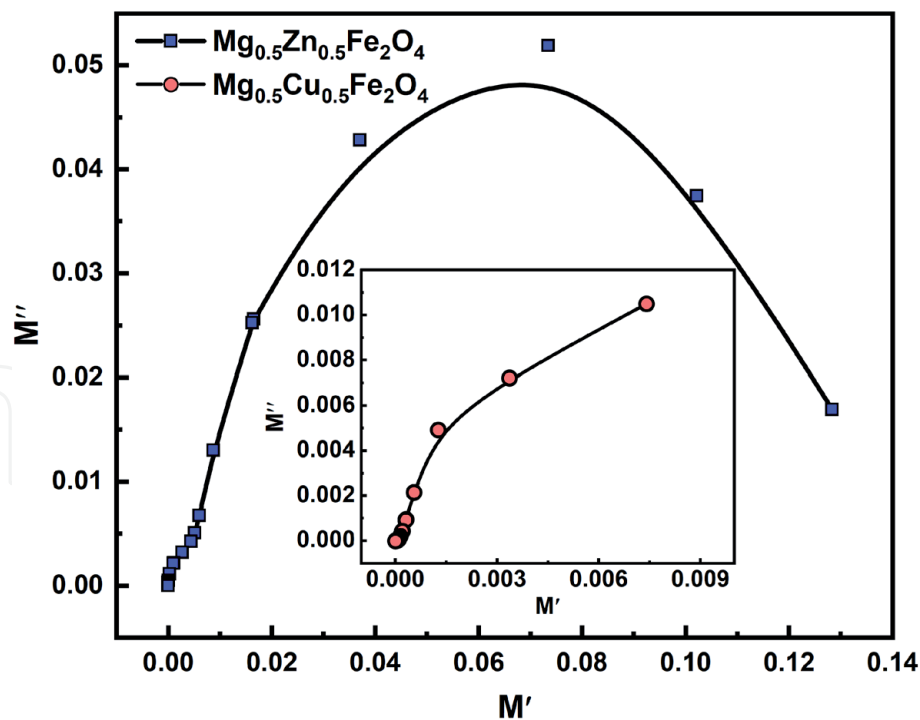


Figure 6.
 Variation of imaginary modulus (M'') as a function of real modulus (M') of $Mg_{0.5}Tm_{0.5}Fe_2O_4$ ($Tm = Zn$ and Cu) ferrites.

values of grain boundaries. Complex modulus analysis is useful when materials have different capacitance [21]. It is confirmed in our M'' versus frequency plot where the grain boundaries are negligible. Even if present, their contribution to the overall capacitance of the material is very small, and does not affect the relaxation process much. The modulus spectrum shows a marked change in its shape/size with Cu ion doping [22].

4. Conclusions

The polycrystalline $Mg_{0.5}Tm_{0.5}Fe_2O_4$ ($Tm = Zn$ and Cu) ferrite samples were successfully prepared using the solid state reaction method. The Rietveld refinement study of XRD reveals that the samples crystallize in cubic spinel structure with the $Fd-3m$ space group. The monoclinic crystal phase of the CuO (space group $C2/c$) compound is seen in $Mg_{0.5}Cu_{0.5}Fe_2O_4$ as a minor secondary phase. It is observed that for both ferrite samples the dielectric constant (ϵ') and dielectric loss ($\tan \delta$) decreases with an increase of frequency and becomes constant at a higher frequency. The value of ϵ' and σ_{ac} are enhanced, whereas the value of $\tan \delta$ decreases for $Mg_{0.5}Cu_{0.5}Fe_2O_4$. The $M'-M''$ plot of $Mg_{0.5}Zn_{0.5}Fe_2O_4$ shows two regions, referring to the grain as well as the grain boundary conducting process. There is no semi-circle type behavior in the $Mg_{0.5}Cu_{0.5}Fe_2O_4$ sample which means that only grain capacitance is dominant and the grain boundary modulus is beyond the measurement scale.

Acknowledgements

UGC-DAE-CSR, as an institute is acknowledged for extending its facilities for sample characterization. Dr. M. Gupta, Dr. D. M. Phase of UGC-DAE-CSR, Indore, India are gratefully acknowledged for measurements and fruitful discussions.

Conflict of interest

The authors declare no conflict of interest.

IntechOpen

Author details

Pallavi Saxena^{1*} and Anand Yadav²

1 Materials Science Laboratory, School of Physics, Vigyan Bhawan, Devi Ahilya University, Khandwa Road Campus, Indore, India

2 Department of Physics, Medi-Caps University, Pigdamber, Indore, India

*Address all correspondence to: pallaviphy12@gmail.com

IntechOpen

© 2021 The Author(s). Licensee IntechOpen. This chapter is distributed under the terms of the Creative Commons Attribution License (<http://creativecommons.org/licenses/by/3.0>), which permits unrestricted use, distribution, and reproduction in any medium, provided the original work is properly cited. 

References

- [1] K. Praveena, K. Sadhana, S. Bharadwaj, and S. R. A. Murthy, J. Magn. Magn. Mater. **321**, 2433 (2009).
- [2] V. Tsakaloudi and V. Zaspalis, J. Magn. Magn. Mater. **400**, 307 (2016).
- [3] Z. H. Zhou, J. M. Xue, H. S. O. Chan, and J. Wang, J. Appl. Phys. **90**, 4169 (2001).
- [4] H. M. Zaki, S. H. Al-Heniti, and T. A. Elmosalami, J. Alloys Compd. **633**, 104 (2015).
- [5] U. Ghazanfar, S. A. Siddiqi, and G. Abbas, Mater. Sci. Eng. B **118**, 84 (2005).
- [6] U. R. Ghodake, N. D. Chaudhari, R. C. Kambale, J. Y. Patil, and S. S. Suryavanshi, J. Magn. Magn. Mater. **407**, 60 (2016).
- [7] M. Ishaque, M. A. Khan, I. Ali, H. M. Khan, M. A. Iqbal, M. U. Islam, and M. F. Warsi, Ceram. Int. **41**, 4028 (2015).
- [8] D. L. Sekulic, Z. Z. Lazarevic, M. V. Sataric, C. D. Jovalekic, and N. Z. Romcevic, J. Mater. Sci. Mater. Electron. **26**, 1291 (2015).
- [9] C. Choodamani, B. Rudraswamy, and G. T. Chandrappa, Ceram. Int. **42**, 10565 (2016).
- [10] P. Scardi, L. B. Mccusker, R. B. Von Dreele, D. E. Cox, and D. Loue, J. Appl. Cryst. (1999). **32**, 36 (1999).
- [11] D. Nath, F. Singh, and R. Das, Mater. Chem. Phys. **239**, 122021 (2020).
- [12] M. Arifuzzamana; and M. B. Hossen;, Results Phys. **16**, 102824 (2020).
- [13] H. Saqib, S. Rahman, R. Susilo, B. Chen, and N. Dai, AIP Adv. **9**, (2019).
- [14] Z. Iwauchi, Jpn. J. Appl. Phys. **10**, 1520 (1971).
- [15] R. C. Kambale, P. A. Shaikh, Y. D. Kolekar, C. H. Bhosale, and K. Y. Rajpure, Mater. Lett. **64**, 520 (2010).
- [16] P. Saxena, P. Choudhary, A. Yadav, B. Dewangan, V. N. Rai, and A. Mishra, Appl. Phys. A **126**, 765 (2020).
- [17] A. Yadav and D. Varshney, J. Supercond. Nov. Magn. **30**, 1297 (2017).
- [18] P. Saxena, P. Choudhary, A. Yadav, V. N. Rai, and A. Mishra, J. Mater. Sci. Mater. Electron. **31**, 12444 (2020).
- [19] P. Saxena, P. Choudhary, A. Yadav, V. N. Rai, M. Varshney, and A. Mishra, J. Mater. Sci. Mater. Electron. **30**, 7292 (2019).
- [20] M. M. N. Ansari, S. Khan, and N. Ahmad, Phys. B Condens. Matter **566**, 86 (2019).
- [21] P. Saxena and D. Varshney, J. Alloys Compd. **705**, 320 (2017).
- [22] E. AlArfaj, S. Hcini, A. Mallah, M. H. Dhaou, and M. L. Bouazizi, J. Supercond. Nov. Magn. **31**, 4107 (2018).